Dalton Transactions

Visible Light Induced Formation of a Tungsten Hydride Complex

Journal:	*Dalton Transactions*
Manuscript ID	DT-ART-11-2022-003675.R1
Article Type:	Paper
Date Submitted by the Author:	02-Feb-2023
Complete List of Authors:	Isaacs, Diane; University of North Carolina, Chemistry Gruninger, Cole; University of North Carolina, Chemistry Huang, Tao; University of North Carolina at Chapel Hill, Chemistry Jordan, Aldo; University of Texas at El Paso, Department of Chemistry and Biochemistry Nicholas, Genique; University of North Carolina, Chemistry Chen, Chun-Hsing; University of North Carolina at Chapel Hill ter Horst, Marc; University of North Carolina, Chemistry Dempsey, Jillian; University of North Carolina, Chemistry

ARTICLE

Visible Light Induced Formation of a Tungsten Hydride Complex

Diane P. Isaacs, [†a] Cole T. Gruninger, [†a] Tao Huang,[a] Aldo M. Jordan[a], Genique Nicholas,[a] Chun-Hsing Chen,[a] Marc A. ter Horst,[a] Jillian L. Dempsey[a]

Received 00th January 20xx,
Accepted 00th January 20xx

DOI: 10.1039/x0xx00000x

When irradiated with blue light in the presence of a Lewis base (L), $[CpW(CO)_3]_2$ undergoes a metal–metal bond cleavage followed by a disproportionation reaction to form $[CpW(CO)_3L]^+$ and $[CpW(CO)_3]^-$. Here, we show that in the presence of pyridinium tetrafluoroborate, $[CpW(CO)_3]^-$ reacts further to form a metal hydride complex $CpW(CO)_3H$. The rection was monitored through in situ photolytic ^1H NMR spectroscopy experiments and the mechanism of light-driven hydride formation was investigated by determining quantum yields of formation. Quantum yields of formation of $CpW(CO)_3H$ correlate with $I^{-1/2}$ (I = photon flux on our sample tube), indicating that the net disproportionation of $[CpW(CO)_3]_2$ to form the hydride precursor $[CpW(CO)_3]^-$ occurs primarily through a radical chain mechanism.

Introduction

Transition metal hydride complexes serve as essential intermediates in a myriad of chemical reactions that produce fuels and commodity chemicals. In particular, transition metal hydride complexes play a key role in a variety of reactions, including hydrogenation catalysis, C-H bond activation, N_2 reduction, and CO_2 reduction reactions.[1–4] The formation of transition metal hydride complexes using visible light energy offers the opportunity to use solar energy to drive many of society's most valuable chemical transformations. Specifically, the chemical bonds formed upon reaction of a transition metal hydride complex with a substrate will encapsulate some of the energy of the photon that initiated the entire process.[5,6] Thus, gaining a better understanding of light-driven hydride formation provides a means to develop future transition metal catalysts for efficient production of solar fuels.

There are two general approaches to initiate the formation of transition metal hydride complexes with light. The first approach utilizes the excitation of a photoreductant or photoacid to drive a proton-coupled electron transfer (PCET) reaction with a ground state transition metal complex to afford the target transition metal hydride complex.[5,6] A handful of examples that make use of photoreductants[3,7] and photoacids[8] to drive the production of transition metal hydride complexes with light have been reported. The second approach employs a photoactive transition metal complex that when excited, reacts with an acid and a reductant in their ground state to generate a transition metal hydride. Examples of coordination complexes which, upon photoexcitation, are reduced and protonated to generate metal hydride complexes are much rarer.[9,10]

$[CpM(CO)_3]_2$ (M = Cr, Mo, W; Cp = cyclopentadienyl) complexes are known to undergo photochemical disproportionation reactions when irradiated with visible light in the presence of Lewis basic ligands (L) to yield monomeric, $18e^-$ disproportionation products $[CpM(CO)_3L]^+$ and $[CpM(CO)_3]^-$.[11–16] Two mechanisms for the photochemical disproportionation of $[CpM(CO)_3]_2$ complexes have previously been considered, a radical chain mechanism (Scheme 1A) and an in-cage disproportionation mechanism (Scheme 1B). Based on bulk photolysis studies of $[CpM(CO)_3]_2$ (M = Mo) varying the identity of the Lewis base and measuring quantum yields, Tyler and coworkers concluded that the disproportionation reaction occurred via a light-initiated radical chain pathway proceeding through a $CpM(CO)_3L^\bullet$ $19e^-$ intermediate.[11–13] In this mechanism, absorption of a visible light photons results in homolysis of the metal-metal σ bond to form two $17e^-$ radical $CpM(CO)_3^\bullet$ complexes (Scheme 1A). The geminate $17e^-$ radical species can quickly recombine,[14] but upon cage escape the $17e^-$ species can diffuse into bulk solution and coordinate a Lewis base (such as an amine, nitrile, or phosphine) to form a highly reducing $19e^-$ radical species $CpM(CO)_3L^\bullet$.[11,17] Electron transfer from this $19e^-$ radical to the parent dimer $[CpM(CO)_3]_2$ generates the $18e^-$ cationic species $[CpM(CO)_3L]^+$ and the reduced dimer $[CpM(CO)_3]_2^{\bullet-}$. Subsequent M–M bond rupture of the anionic dimer produces the $18e^-$ anion $[CpM(CO)_3]^-$ and another equivalent of the $17e^-$ radical $CpM(CO)_3^\bullet$.[11] Tyler's observation of quantum yield measurements greater than unity (under some conditions) and observed correlations between quantum yield and $I^{-1/2}$ (I = photon flux on the sample) are consistent with this radical chain mechanism.[11]

Transient absorption experiments by Cahoon et al. on the picosecond timescale provide evidence for in-cage disproportionation of the $17e^-$ radicals $CpM(CO)_3^\bullet$ (M = W) formed upon photo-induced homolysis of the $[CpM(CO)_3]_2$

[a] Department of Chemistry, University of North Carolina at Chapel Hill, Chapel Hill, North Carolina 27599-3290, United States

† These authors contributed equally.

Electronic Supplementary Information (ESI) available: ^1H NMR spectrum of control experiments, concentration profiles for in situ ^1H NMR spectroscopy experiments, acid concentration studies, crystallographic data and details, calibration curve for the photolysis lamp, and computational details (PDF). See DOI: 10.1039/x0xx00000x

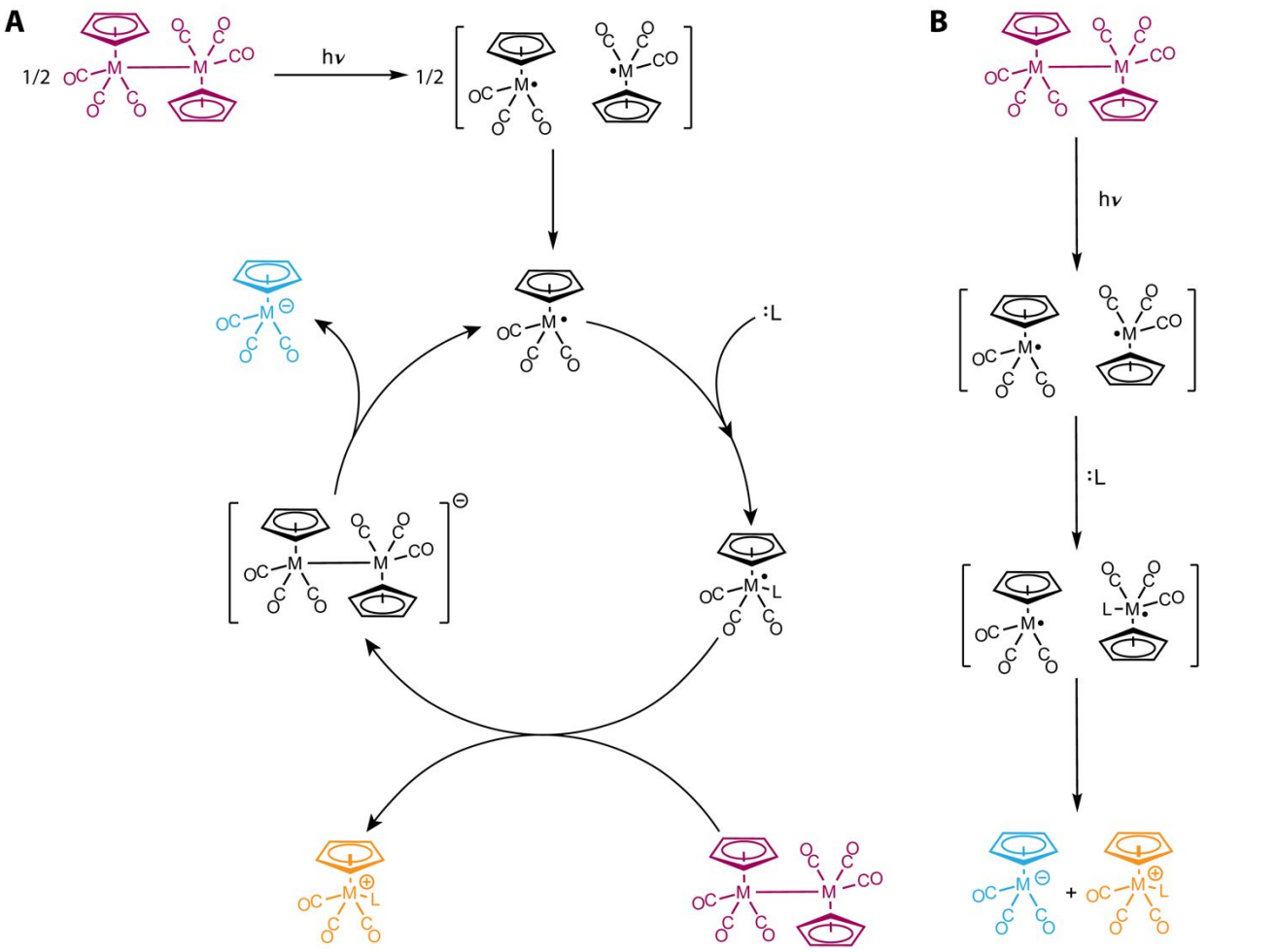

Scheme 1 (A) Photochemical disproportionation by a radical chain mechanism in the presence of a Lewis base (L). (B) In-cage photochemical disproportionation mechanism. Brackets [ ] denote the presence of the solvent cage.

dimer (Scheme 1B).[14,15,18] Coordination of a phosphine or phosphite ligand to one of the caged radicals yields the 19 e⁻ intermediate $CpM(CO)_3L^{\bullet}$ which subsequently transfers an electron to the co-caged 17 e⁻ radical $CpM(CO)_3^{\bullet}$, forming the 18 e⁻ species $[CpM(CO)_3L]^+$ and $[CpM(CO)_3]^-$. Subsequent cage escape separates the charged products.[14] Additionally, Cahoon et al. found that when L was a strong donor and in high concentration, 2 equivalents of $CpM(CO)_3L^{\bullet}$ form in the solvent cage.[14]

Intrigued by the light-driven production of $[CpM(CO)_3]^-$, we hypothesized that under the appropriate conditions, this anionic species would react with a proton source to produce the corresponding $CpM(CO)_3H$ species (Scheme 2). Indeed, we find that photolysis of a dimeric tungsten complex $[CpW(CO)_3]_2$ in the presence of pyridinium tetrafluoroborate, using acetonitrile (CH_3CN) as both the Lewis base and solvent, leads to the near quantitative formation of the tungsten hydride complex $CpW(CO)_3H$ (with 1 equiv. $CpW(CO)_3H$ generated per $[CpW(CO)_3]_2$ dimer). The photolysis reaction was monitored *in situ* using ^1H NMR spectroscopy; analysis shows that the overall rate law is acid concentration independent. Quantum yield measurements as a function of photon flux suggest the primary reaction pathway toward tungsten hydride formation is a radical chain mechanism likely accessed by the 19 e⁻ radical, $CpW(CO)_3L^{\bullet}$, that escapes the solvent cage, providing new insight to the dominant mechanism of radical chain disproportionation.

Experimental

General Considerations

All syntheses were performed under N_2, either on a Schlenk line or in an inert-atmosphere glovebox. Synthesis of $CpW(CO)_3H$,[19] triphenylmethyl radical[20] (Moses Gomberg's dimer), and pyridinium tetrafluoroborate[21] were performed according to literature methods. Acetonitrile (Fisher Scientific, HPLC grade, > 99.9 %), diethyl ether (Fisher Scientific, > 99 %), and dichloromethane (Fischer Scientific, > 99 %) were degassed with argon and dried using a Pure Process Technology solvent system. Deuterated acetonitrile (Cambridge Isotope Laboratories, > 99.8 %) was stirred over CaH_2 for 24 hours,

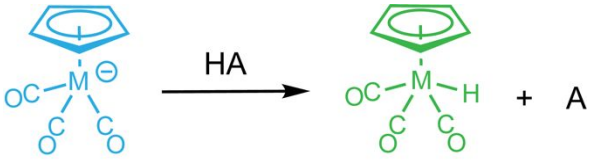

Scheme 2 Protonation of $[CpW(CO)_3]^-$ by HA to form $CpW(CO)_3H$ and A^-.

degassed using a freeze-pump-thaw technique, and stored under the inert-atmosphere glovebox. All NMR spectra were recorded on either a VIII 500 MHz spectrometer with a standard 5mm broad band probe (characterization) or a Bruker NEO 600 MHz spectrometer with a QNP cryoprobe or with a BBFO probe (reaction monitoring). ^{1}H NMR spectra were acquired using an externally calibrated 30 degree pulse width and referenced to residual proteo solvent chemical shifts. UV–vis absorption measurements were taken on an Agilent Cary 60 UV–vis spectrophotometer using 1 cm path length quartz cuvettes.

Synthesis of $[CpW(CO)_3]_2$

Preparation of $[CpW(CO)_3]_2$ was adapted from literature procedures.[22–24] Within an inert atmosphere glovebox, in separate scintillation vials, recrystallized $CpW(CO)_3H$ (0.140 g, 0.421 mmol, 2.05 equiv) and trityl bromide (0.100 g, 0.205 mmol, 1 equiv) were dissolved in neat diethyl ether and then combined to yield a cloudy, crimson red solution. After stirring for 30min, the diethyl ether solvent was removed by vacuum and the resulting red powder was rinsed several times with diethyl ether for purification. (0.079 g, 0.119 mmol, 61% yield). ^{1}H NMR (500 MHz, CD_3CN) δ 5.56 (s,10H, gauche), 5.46 (s, 10H, anti). The anti and gauche isomers are present in a 5:3 ratio.

Synthesis of $[CpW(CO)_3(NCCH_3)][PF_6]$

Preparation of $[CpW(CO)_3(NCCH_3)][PF_6]$ was adapted from literature procedures.[23,25,26] Within the inert atmosphere glovebox, recrystallized $CpW(CO)_3H$ (0.080g, 0.24 mmol, 1.1 equiv), 1 equiv.), and acetonitrile (5 equiv.) were combined in dichloromethane. A solution of tritylium hexafluorophosphate (0.085g, 0.22 mmol, 1 equiv.) in dichloromethane, was added to the $CpW(CO)_3H$ solution to yield a bright orange solution instantaneously. After stirring for 20 min, solvent was removed by vacuum. The resulting orange powder was rinsed several times and subsequently recrystallized in dichloromethane and diethyl ether. Bright orange crystals suitable for X-ray diffraction were obtained (0.093 g, 0.18 mmol, 80% yield). ^{1}H NMR (500 MHz, CD_3CN) δ 6.05 (s, 5H), 2.57 (s, 3H).

Synthesis of $Na[CpW(CO)_3]$

Preparation of $Na[CpW(CO)_3]$ was modified from literature procedures.[27,28] $CpW(CO)_3H$ (0.050 g, 0.15 mmol, 1.2 equiv) and sodium hydride (0.003 g, 0.013 mmol, 1 equiv) were dissolved in neat acetonitrile to yield a transparent and colorless solution. After stirring for 25 min, solvent was removed by vacuum. The resulting white powder was washed 3 times with diethyl ether (0.038 g, 0.11 mmol, 76 % yield) ^{1}H NMR (500 MHz, CD_3CN) δ 5.11 (s, 5H).

Density Functional Theory Calculations

All DFT and TD-DFT calculations were carried out using the program package Gaussian[29,30] and the B3LYP density functional.[30] The basis set used for all other atoms besides tungsten atoms was 6-31G**.[31] For the two tungsten atoms, the LANL2DZ basis set, which includes a relativistic effective core potential, was used for all calculations.[32] Hessian matrices were calculated at each stationary point in order to ensure that true minima along the potential energy hypersurfaces had been found.

In situ NMR monitoring of photoreactions

To monitor photolysis *in situ*, we utilized a New Era photoNMR sampling device equipped with a concentric tube whose interior held a heat resistant, 0.6 mm polymer optical fiber connected to a Prizmatrix ultra high brightness LED lamp centered at a wavelength of 450 nm (FWHM = 25 nm). The fiber coating was removed for the length for the NMR tube and the fiber itself scuffed with sandpaper only for the region of the detection coil in the probe; this allows the entire length of the sampling device to be irradiated. The light intensity of the LED light is modulated using an analog input – a ninety-nine turn dial – for precise power control with LED power stabilizer. The dial was set to a power setting of 3 for all in situ photoreactions. All samples were prepared in a nitrogen filled glovebox as 1 mL solutions with biphenyl as an internal standard (0.130 mmol, 20 mg) and the reagents specific to that reaction. Samples containing $[CpW(CO)_3]_2$ were filtered to remove any undissolved dimer. A New Era photoNMR sampling device was loaded with 0.6 mL of solution. One spectrum was obtained prior to turning the light on, followed by 59 single scan spectra with the light on, unless specified otherwise. The D_1 time for all experiments was set to 60 s with a fixed delay of 0 s between scans.

Quantum Yield Measurements

All quantum yield measurements were completed with a ThorLabs multi-wavelength LED lamp (455nm, FWHM = 18 nm) set-up on the lab bench. The lamp was turned on an hour before irradiation to allow the power to stabilize. All samples were prepared in a nitrogen filled glovebox. 1,3,5-trimethoxybenzene (TMB, 0.0375 g, 0.223 mmol) and $[pyridinium][BF_4]$ (0.0375 g, 0.201 mmol) were weighed out in a 3 mL volumetric flask and dissolved in CD_3CN that had been dried over calcium hydride to remove any residual water present. Approximately 10 mg of $[CpW(CO)_3]_2$ was weighed out in a vial. The TMB and pyridinium solution was added to the vial with $[CpW(CO)_3]_2$ and was dissolved until saturation. The resulting solution was filtered into a clean vial to remove any undissolved $[CpW(CO)_3]_2$. Each of 3 J. Young tubes was loaded with 700 µL of solution and immediately covered with aluminum foil to protect them from ambient light. A ^{1}H-NMR spectrum was acquired for each sample prior to irradiation with the LED lamp. Samples were placed 3.5 cm distance away from the lamp and irradiated with 455 nm light for 1-4 min depending on the set intensity of the irradiated light. A second ^{1}H-NMR spectrum was acquired after irradiation. The delay time for ^{1}H NMR spectra was 45s. The internal standard, TMB was used to compute concentrations of $[CpW(CO)_3]_2$ and $CpW(CO)_3H$ before and after irradiation. Quantum yields were computed using the following equation:

$$\Phi = \frac{Moles\ of\ WH}{I_\lambda \cdot t \cdot a \cdot (1 - 10^{-A_\lambda})} \quad (1$$

Where I_λ is the photon flux of the 455 nm ThorLabs LED lamp source on our sample tube (mol photon s^{-1}) at a given current output determined by actinometry with potassium ferrioxalate (See Supporting Information for additional details), t is time of irradiation, and A_λ is the absorbance of the sample at the irradiation wavelength (ε_{455} = 1240 M^{-1} cm^{-1}).

Results and discussion

Synthesis of $[CpW(CO)_3]_2$, $CpW(CO)_3H$, and $[CpW(CO)_3(NCCH_3)]^+$

$CpW(CO)_3]_2$ was synthesized as previously reported.[22–24] Based on previous work investigating the photochemistry of$[CpM(CO)_3]_2$ (M = Cr, Mo, W) and the work reported herein, the anticipated products of the photolysis of $[CpW(CO)_3]_2$ in the presence of a proton source are $CpW(CO)_3H$ and $[CpW(CO)_3(NCCH_3)]^+$. Thus for comparison purposes, authentic samples of $CpW(CO)_3H$ and $[CpW(CO)_3(NCCH_3)]^+$ were prepared.[19,25,26] $[CpW(CO)_3]_2$, $CpW(CO)_3H$ and $[CpW(CO)_3(NCCH_3)]^+$ were all characterized by ^1H NMR spectroscopy to confirm product identity. $[CpW(CO)_3]_2$ has a diagnostic feature for the cyclopentadienyl ring, with anti (5.46 ppm) and gauche (5.56 ppm) isomers observed in a 5:3 ratio. The Cp resonance for $CpW(CO)_3H$ is observed downfield of the dimer (5.63 ppm) and the species also has a diagnostic resonance for the hydride (-7.44 ppm). For comparison, the Cp peak of $[CpW(CO)_3(NCCH_3)]^+$ is downfield of the dimer and the hydride (6.05 ppm). X-ray quality crystals of $[CpW(CO)_3(NCCH_3)]^+$ (Table S1) were obtained by recrystallization in dichloromethane and diethyl ether. Structural characterization confirms identity of this cationic product (Figure 1).

Next, the stability of $[CpW(CO)_3(NCCH_3)]^+$ under photolysis conditions was interrogated. Upon irradiation (λ_{ex} = 450 nm, 30 min) of isolated $[CpW(CO)_3(NCCH_3)]^+$, the CO loss product, $[CpW(CO)_2(NCCH_3)_2]^+$ is observed with diagnostic resonances for the cyclopentadienyl ligand (6.01 ppm) and the bound CH_3CN (2.58 ppm) (Figure S2).

Optical transitions of $[CpW(CO)_3]_2$

The UV-Vis absorption spectrum of $[CpW(CO)_3]_2$ exhibits two absorption bands, one at 488 nm (ε = 2017 M^{-1} cm^{-1}) and one at 356 nm (ε = 15791 M^{-1} cm^{-1}) (Figure 2). Wrighton and Ginley[33] assigned these transitions as $d\pi \rightarrow \sigma^*$ and $\sigma \rightarrow \sigma^*$ transitions, respectively, similar to assignments of $[M(CO)_5]_2$ (M = Mn, Re) by Levenson, Gray, and Ceasar.[34] Time-dependent density functional theory (TD-DFT) calculations of $[CpW(CO)_3]_2$ were used to calculate excitations for $[CpW(CO)_3]_2$ in acetonitrile using implicit solvation (Figure 2). The dominant low energy feature at 488 nm is attributed to a $d\pi \rightarrow \sigma^*$ transition, and the intense absorption feature at 356 nm is best characterized by a $\sigma \rightarrow \sigma^*$ transition, in agreement with Wrighton and Ginely's original assignments. Both transitions populate the σ^* anti-bonding orbital, promoting W-W bond homolysis, in agreement with experimental results.[15]

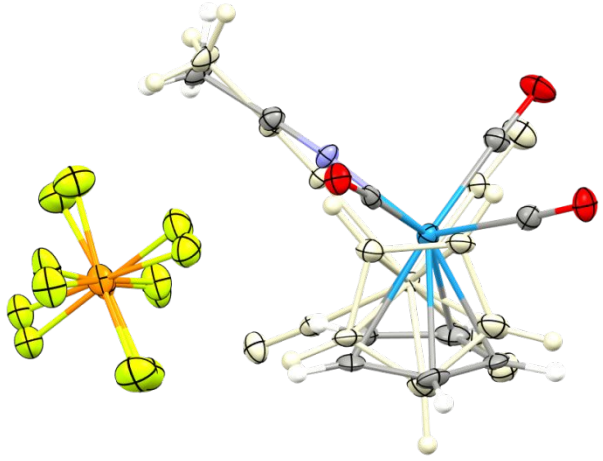

Fig 1 Molecular structure of the asymmetric unit of $[CpW(CO)_3NCCH_3][PF_6]$ with ellipsoids drawn at 50% probability. Blue, purple, red, gray, orange, yellow, and white atoms correspond to W, N, O, C, P, F, and H respectively. The minor component of the complex was colored with white for clarity. Solvent molecules omitted for clarity.

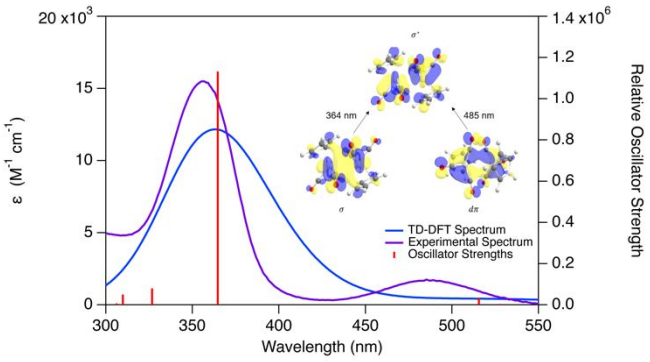

Fig 2 Experimental and calculated UV-vis absorption spectra of $[CpW(CO)_3]_2$. Experimental spectrum recorded in CH_2Cl_2.

Light-driven formation of $CpW(CO)_3H$

Photolysis of the $[CpW(CO)_3]_2$ dimer in the presence of excess pyridinium tetrafluoroborate ($[PyH][BF_4]$) using a 455 nm LED lamp generates $CpW(CO)_3H$ and a mixture of the cationic products $[CpW(CO)_3(NCCH_3)]^+$ and $[CpW(CO)_2(NCCH_3)_2]^+$, as quantified by ^1H NMR spectroscopy (Figure 3). Comparison to authentic samples of $CpW(CO)_3H$, $[CpW(CO)_3(NCCH_3)]^+$, and $[CpW(CO)_2(NCCH_3)_2]^+$ confirms product identity.

Real-time kinetic data for the photolysis of $[CpW(CO)_3]_2$ in the presence of $[PyH][BF_4]$ were obtained using a New Era photoNMR tube with an LED light source introduced to the tube with a fiber optic cable that enables *in situ* NMR monitoring of photoreactions (λ_{ex} = 450 nm). The concentrations of $[CpW(CO)_3]_2$, $CpW(CO)_3H$, $[CpW(CO)_3(NCCH_3)]^+$, and $[CpW(CO)_2(NCCH_3)_2]^+$ were monitored over the photolysis period with reference to the internal standard, biphenyl. The decay of the reactant and formation of the product are observed to occur with first-order kinetics (Figure 4).

There are no reaction intermediates detected via ^1H NMR upon photolysis of $[CpW(CO)_3]_2$ in the presence of $[PyH][BF_4]$. This observation suggests that on the NMR timescale, $[CpW(CO)_3]^-$ reacts rapidly with acid to form $CpW(CO)_3H$, as

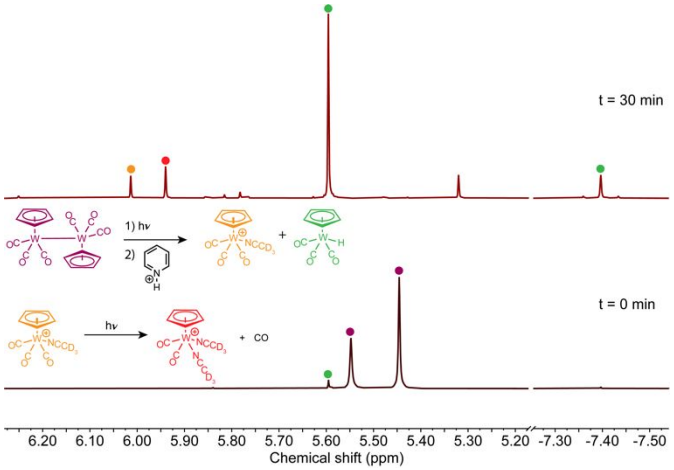

Fig 3 (Bottom) ^1H NMR spectrum of $[CpW(CO)_3]_2$ (1.66 mM) with $[PyH][BF_4]$ (80.4 mM) in CD_3CN before photolysis. (Top) ^1H NMR spectrum after 30 min. photolysis (λ_{ex} = 455 nm). D_1 for ^1H NMR was 60s.

anticipated. These data, along with the first-order kinetics observed for both $[CpW(CO)_3]_2$ consumption and $CpW(CO)_3H$ formation, suggest that the rate-determining step is not $[CpW(CO)_3]^-$ protonation, but a step involved in the disproportionation reaction. To examine this hypothesis further, photolytic reaction kinetics of $[CpW(CO)_3]_2$ were measured at 62.4, 67.9, 131, and 264 mM $[PyH][BF_4]$ at a fixed photon intensity (Figure S9). Initial rates of $CpW(CO)_3H$ formation were determined to be independent of acid concentration, further supporting the conclusion that the rate limiting step for $CpW(CO)_3H$ formation is not $[CpW(CO)_3]^-$ protonation (Figure S9).

Quantifying and Understanding Reaction Product Yields

A 30 min. bulk photolysis (λ = 455 nm) of $[CpW(CO)_3]_2$ with $[PyH][BF_4]$ generates $CpW(CO)_3H$ in 110% yield (Figure 3), determined via reference of the ^1H NMR signals to an internal standard. The observed yield of 110 % is greater than anticipated for disproportionation of the radical species followed by protonation of the resulting $[CpW(CO)_3]^-$, indicating a distinct pathway to form $CpW(CO)_3H$ exists outside those shown in Schemes 1 and 2. Further, the disproportionation mechanism predicts the combined yield of the cationic products $[CpW(CO)_3(NCCH_3)]^+$ and $[CpW(CO)_2(NCCH_3)_2]^+$ should also yield 100% assuming no competing pathways are present. However, their combined yield is only 32.9%.

The observation of a $CpW(CO)_3H$ yield greater than unity suggests that additional $[CpW(CO)_3]^-$ is formed beyond the 1 equiv. produced from disproportionation. Further, our finding

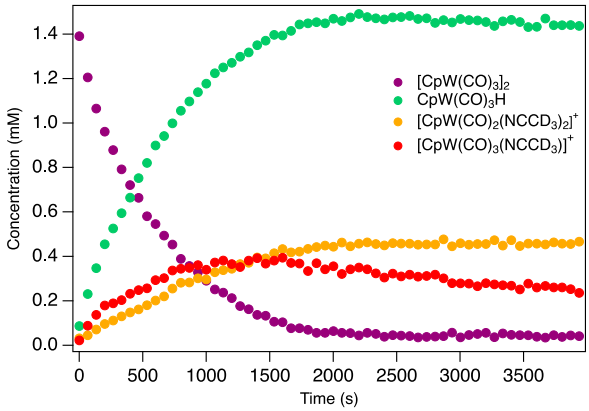

Fig 4 Concentrations of $[CpW(CO)_3]_2$ (maroon), $CpW(CO)_3H$ (green), $[CpW(CO)_3)(NCCH_3)]^+$ (orange), and $[CpW(CO)_2(NCCH_3)_2]^+$ (red) for the reaction of the $[CpW(CO)_3]_2$ with 67.9 mM $[PyH][BF_4]$ under continuous photolysis conditions using the Prizmatix 450 nm LED lamp at an intensity setting of 3. Concentrations are computed by ^1H NMR integration with reference to biphenyl as an internal standard. The experiment was collected as 60 single scan spectra where D_1 = 60 s and there is a 0 s fixed delay between scans.

that the cationic species $[CpW(CO)_3(NCCH_3)]^+$ and $[CpW(CO)_2(NCCH_3)_2]^+$ are formed in sub stoichiometric yield suggests these products react further under photolysis with $[PyH][BF_4]$ present. We hypothesized a fraction of $[CpW(CO)_3(NCCH_3)]^+$ undergoes disproportionation under photolysis conditions to produce tungsten oxide or another highly oxidized species and $[CpW(CO)_3]^-$. The $[CpW(CO)_3]^-$ formed will react with $[PyH][BF_4]$ to form $CpW(CO)_3H$. This pathway would lead to the observed $CpW(CO)_3H$ yields of greater than 100% and lower the observed yield of the cation products. Indeed, *in situ* photolysis of $[CpW(CO)_3(NCCH_3)]^+$ in the presence of $[PyH][BF_4]$ shows some conversion to $CpW(CO)_3H$ (Figure S7).

While the observed conversion of $[CpW(CO)_3(NCCH_3)]^+$ to $CpW(CO)_3H$ (along with co-formation of an oxidized species) upon photolysis in the presence of $[PyH][BF_4]$ explains some of the loss of tungsten products in the bulk photolysis of $[CpW(CO)_3]_2$ with $[PyH][BF_4]$ (λ = 455nm), it cannot account for all of the missing tungsten species. When 1.2 x 10^{-3} mmol of $[CpW(CO)_3]_2$ (2.4 x 10^{-3} mmol of W atoms) are subjected to photolysis in the presence of acid (Figure 3), 1.3 x 10^{-3} mmol of $CpW(CO)_3H$, 0.16 x 10^{-3} mmol of $CpW(CO)_3(NCCH_3)]^+$, 0.23 x 10^{-3} mmol of $[CpW(CO)_2(NCCH_3)_2]^+$ are formed, indicating a net loss of 0.62 x 10^{-3} mmol tungsten-based species (based on tungsten atom economy). To understand if there are other pathways that lead to loss of detectable tungsten cyclopentadienyl compounds, $CpW(CO)_3(NCCH_3)][PF_6]$ and $CpW(CO)_3H$ were individually irradiated in the NMR LED photoreactor in the absence of acid while ^1H NMR spectra were simultaneously recorded at prescribed time points. For $[CpW(CO)_3(NCCH_3)][PF_6]$ (5.1 x 10^{-3} mmol), there is a net loss of 0.36 x 10^{-3} mmol of expected tungsten-based species to unidentified decomposition products in the Cp region of the ^1H NMR in the photolysis was observed (Figure S6), while for $CpW(CO)_3H$ (5.4 x 10^{-3} mmol) a 0.22 x 10^{-3} mmol loss was observed (Figure S8). Additionally, when $[CpW(CO)_3(NCCH_3)][PF_6]$ is irradiated in the NMR LED photoreactor in the presence of acid, $[CpW(CO)_3(NCCH_3)]^+$ (2.2 x 10^{-3} mmol),to 0.040 x 10^{-3} mmol of $CpW(CO)_3H$ is formed and 0.55 x 10^{-3} mmol of the starting $[CpW(CO)_3(NCCH_3)]^+$ is lost, presumably to form unidentified decomposition products (Figure S7). The mass loss and observation of decomposition products by ^1H NMR spectroscopy indicates that these products have limited photostability.

Investigating Stability of Reactants and Products

To ensure thermal decomposition was not contributing to the observed reactivity, $[CpW(CO)_3]_2$ was simultaneously heated in the presence of [Py-H][BF_4] and the absence of light ($[CpW(CO)_3]_2$ left in ambient light reacts slowly, Figure S3). The sample was heated at 80° C for 12 h, ^1H NMR spectrum indicated no reaction and retention of $[CpW(CO)_3]_2$. This data confirms that photons, not incidental heating, are responsible for dimer disproportionation and subsequent hydride formation (Figure S1). Notably, no carbonyl ligands are lost under these conditions.

The photolysis of $[CpW(CO)_3]_2$ (1.4 x 10^{-3} mmol, 2.8 x 10^{-3} mmol W atoms) was also conducted in the absence of acid to better understand the reaction before protonation and to ensure that $CpW(CO)_3H$ is protonated by $[PyH][BF_4]$ and not an adventitious proton source. When the sample was irradiated for 30 mins with 455 nm light, the anticipated products $[CpW(CO)_3(NCCH_3)]^+$, $[CpW(CO)_2(NCCH_3)_2]^+$ and $[CpW(CO)_3]^-$ were detected via ^1H NMR spectroscopy (Figure S4).

Surprisingly, $CpW(CO)_3H$ was also observed. We determined that $[CpW(CO)_3]^-$, $[CpW(CO)_3(NCCH_3)]^+$, $[CpW(CO)_2(NCCH_3)_2]^+$, and $CpW(CO)_3H$ are present in the photolysis reaction mixture in 0.65 x 10^{-3}, 0.16 x 10^{-3}, 0.21 x 10^{-3}, and 0.50 x 10^{-3} mmol yields respectively and 0.26 x 10^{-3} mmol of $[CpW(CO)_3]_2$ left unreacted and 1.0 x 10^{-3} mmol W atoms unaccounted for. This yields a net ratio of the tungsten anion plus hydride to cationic species of 3.1 : 1. The sub stoichiometric yield of cationic products is qualitatively consistent with what is observed in the presence of $[Py\text{-}H][BF_4]$. The appearance of $[CpW(CO)_3]^-$ in the ^1H NMR spectrum in the absence of acid after irradiation confirms that $[CpW(CO)_3]^-$ is a reaction intermediate and further supports that conclusion that protonation is fast and quantitative when $[Py\text{-}H][BF_4]$ is present. The surprising observation of $CpW(CO)_3H$ as a photolysis product in the absence of acid suggests an adventitious proton source is present that protonates the anion. While all solvents were dried over calcium hydride and stored over sieves, adventitious water is likely still present at low concentrations and was hypothesized to be the proton source for experiments conducted in the absence of $[PyH][BF_4]$. To confirm our hypothesis, a control experiment was conducted in in which $[CpW(CO)_3]_2$ was photolyzed with intentionally added water (1.1 mM). Compared to the same experiment in the absence of water or acid, an increase in conversion of $[CpW(CO)_3]_2$ to $CpW(CO)_3H$ is observed, from 5.4% with no proton source added to 13% with water added (Figure S5). Additionally, the amount of $[CpW(CO)_3]^-$ present after irradiation decreases from 4.9% to 2.8%, supporting the conclusion that water can act as a proton source in this reaction. While the conversion of $CpW(CO)_3^-$ to $CpW(CO)_3H$ via the presumptive protonation by adventitious water is surprisingly high in this 30 min photolysis, the observation of decomposition products visible in the Cp region of the ^1H NMR spectrum suggests that photolysis in the presence of pyridinium leads to cleaner conversion with less side reactivity.

Intensity (mol photons $s^{-1}cm^{-2}$)	Quantum Yield
6.18 x 10^{-9}	0.026
7.67 x 10^{-9}	0.041
1.07 x 10^{-8}	0.045
1.36 x 10^{-8}	0.060
1.66 x 10^{-8}	0.064
1.96 x 10^{-8}	0.066
2.26 x 10^{-8}	0.068
2.85 x 10^{-8}	0.068
3.45 x 10^{-8}	0.070

Table 1 Quantum yields of $CpW(CO)_3H$ formation as a function of light intensity.

Probing the Mechanism of Disproportionation

Cahoon et al. used ultrafast transient absorption spectroscopy to establish that the extent $CpW(CO)_3^\bullet$ radicals disproportionate within the solvent cage depends on both the Lewis base identity and its concentration (Scheme 1B), acknowledging these conclusions are restricted to the processes that occur within 150 picoseconds after excitation.[14,15,18] This work also established that for very strong Lewis bases, the equilibrium between $CpW(CO)_3^\bullet$ and $CpW(CO)_3^\bullet L$ favors the 19 e^- species so that any 17 e^- radicals not consumed by disproportionation are converted to $CpW(CO)_3^\bullet L$. While Cahoon's study focused on phosphine and phosphite ligands, acetonitrile is reported to have even stronger donating ability for this family of complexes.[35] Separately, Tyler and coworkers utilized the observation of quantum yields of greater than unity (observed under some conditions) and observed correlations between quantum yield and $I^{-1/2}$ (I = photon flux on the sample) to support their assignment of a radical chain mechanism for the homolysis of $[CpM(CO)_3]_2$ complexes.[11,16,35,36] In this limiting mechanism, radicals that escape the solvent cage before disproportionation drive a radical chain reaction (Scheme 1A). While Tyler's reports suggest it is the 17 e^- radicals $CpM(CO)_3^\bullet$ that escape the solvent cage, and then bind a Lewis base in solution to form the highly reducing 19 e^- radical $CpM(CO)_3L^\bullet$ (that then reduces unreacted $[CpM(CO)_3]_2$), we suggest here that L binds to the $CpW(CO)_3^\bullet$ radicals in the solvent cage forming the 19 e^- radicals, $CpW(CO)_3L^\bullet$, invoked by Cahoon's findings (that strong donors in high concentration can bind to both 17 e^- radicals in the solvent cage) and that these 19 e^- radicals can also provide entry to this cycle (Scheme 3). This revises the radical chain pathway initially proposed by Tyler, as entry to the radical chain cycle via a 19 e^- radical has not previously been postulated.

In our work, the disproportionation product $[CpW(CO)_3]^-$ is the critical precursor to $CpW(CO)_3H$. Eager to interrogate the underlying mechanism of this photon-driven hydride formation reaction, we determined quantum yields for $CpW(CO)_3H$ formation upon photolysis of $[CpW(CO)_3]_2$ with 455 nm light. Quantum yields were measured at 9 different light intensities ranging from 6.18 x 10^{-9}– 3.45 x 10^{-8} mol photons s^{-1} cm^{-2}, with light intensities determined for each setting of the LED power

Scheme 3 Photochemical disproportionation can occur by an in-cage disproportionation mechanism (1) and a radical chain mechanism. Entry points to the radical chain mechanism are possible upon cage escape of either 17 e⁻ (2) or 19 e⁻ (3) radicals. Brackets [ ] denote the presence of the solvent cage.

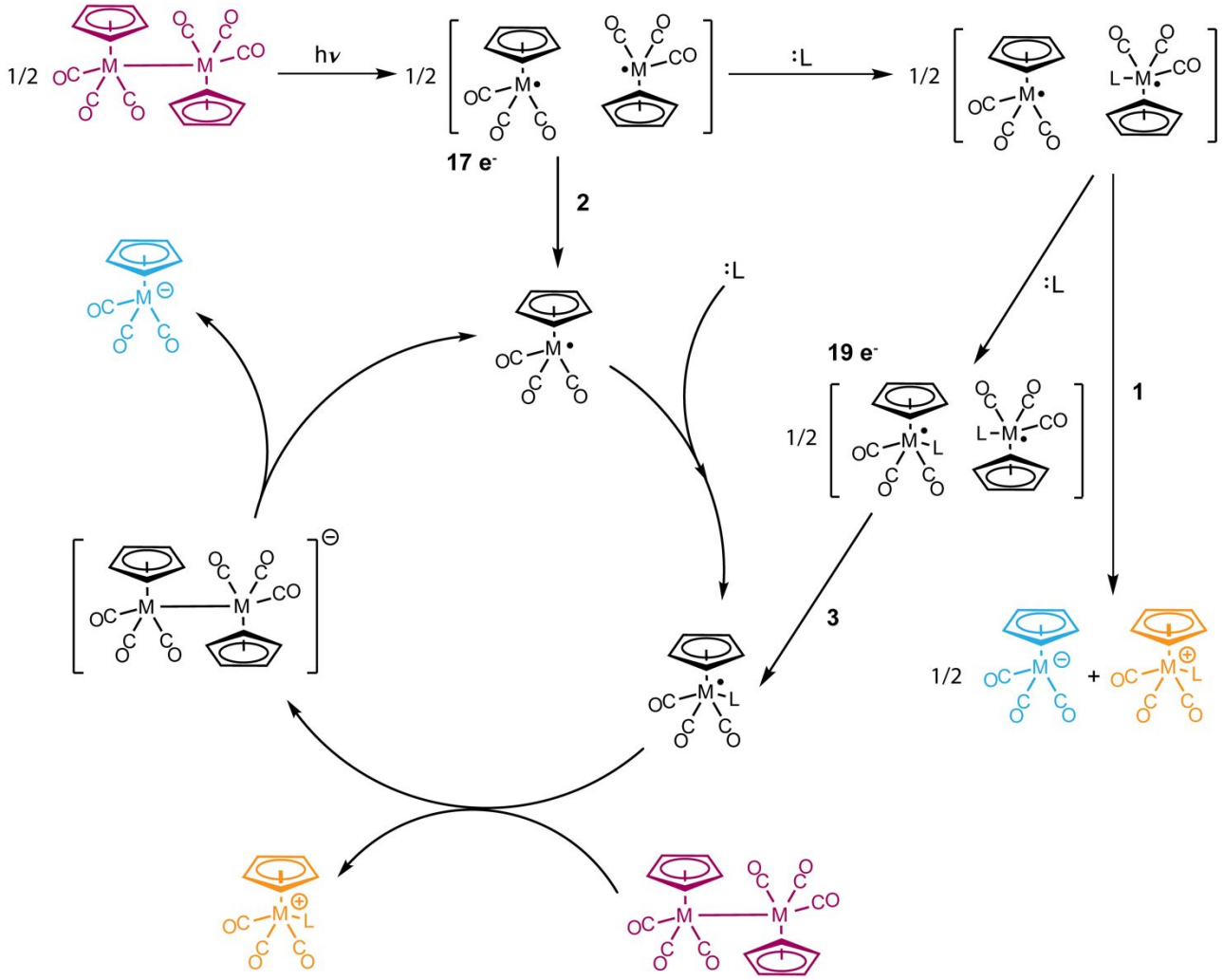

supply using actinometry (see Supporting Information for details). These data (Table 1) show that quantum yields for $CpW(CO)_3H$ formation range from 2.6–7.0%. While Tyler has reported quantum yields of greater than unity for the disproportionation of $[(MeCp)Mo(CO)_3]_2$ (MeCp = η^5-$CH_3C_5H_4$) in acetone, it's notable his reported quantum yields for the same species in acetonitrile are more consistent with what we observe for the $CpW(CO)_3H$ formation at similar photon fluxes (Φ = 0.02 at 1.77 x 10^{-8} mol photon s^{-1}).[13] A more telling test to assess the mechanism is to plot the quantum yield as a function of photon flux (Figure S13). We observed a correlation between quantum yield and the inverse square root of photon flux on our sample tube ($I^{-1/2}$), consistent with what is predicted by the steady state approximation for the radical chain mechanism (see Supporting Information).

The correlation observed between quantum yield and $I^{-1/2}$, together with Cahoon's observation that strong donor ligands drive the formation of the highly reducing 19 e⁻ species $CpW(CO)_3$•L, suggests that the majority of the disproportionation product $[CpW(CO)_3]^-$ is generated through the radical chain mechanism, which can be initiated by either a 17 e⁻ or 19 e⁻ radical (Scheme 3). Any $[CpW(CO)_3]^-$ formed by disproportionation in turn reacts with $[PyH][BF_4]$ to form $CpW(CO)_3H$ (Scheme 2).

Conclusions

In summary, we have demonstrated that the visible-light photolysis of the $[CpW(CO)_3]_2$ dimer, in the presence of pyridinium tetrafluoroborate acid, results in $CpW(CO)_3H$ formation. Reaction yields for $CpW(CO)_3H$ higher than 100% arise from a parallel redox-based reaction pathway. The photolysis of $[CpW(CO)_3]_2$ was monitored in situ using a specialized NMR photolysis reaction setup, where $CpW(CO)_3H$ formation was observed to be independent of acid concentration. Quantum yield measurements of $CpW(CO)_3H$ formation show a correlation with $I^{-1/2}$, suggesting that the net disproportionation of $[CpW(CO)_3]_2$ occurs primarily through a radical chain mechanism. Identifying methods utilizing light to form metal hydride will help drive forward renewable energy effort to create and store renewable fuels.

Conflicts of interest

There are no conflicts to declare.

Acknowledgements

This work was supported by the National Science Foundation (CHE-1954868). J.L.D. acknowledges support from a Packard Fellowship for Science and Engineering. G.N. acknowledges support from the NSF SUROC REU Program (CHE-1460874). We thank Prof. Alexander J. M. Miller for providing access to photolysis equipment. This work made use of an X-ray crystal diffractometer supported by the National Science Foundation under Grant No. (CHE-2117287). We thank the University of North Carolina's Department of Chemistry NMR Core Laboratory for the use of their NMR spectrometers and Dr. Nuwanthika Kumarage for her assistance with NMR spectroscopy. This work made use of an NMR spectrometer supported by the National Science Foundation (CHE-0922858). We thank Quinton Bruch for insightful discussions and experimental assistance with quantum yield measurements.

References

1 Perutz, R. N.; Procacci, B. Photochemistry of Transition Metal Hydrides. *Chem. Rev.* 2016, **116**, 8506–8544.
2 Dempsey, J. L.; Brunschwig, B. S.; Winkler, J. R.; Gray, H. B. Hydrogen Evolution Catalyzed by Cobaloximes. *Acc. Chem. Res.* 2009, **42** , 1995–2004.
3 Teets, T. S.; Nocera, D. G. Photocatalytic Hydrogen Production. *Chem. Commun.* 2011, **47** , 9268–9274.
4 Concepcion, J. J.; House, R. L.; Papanikolas, J. M.; Meyer, T. J. Chemical Approaches to Artificial Photosynthesis. *Proc. Natl. Acad. Sci. U. S. A.* 2012, **109**, 15560–15564.
5 Lennox, J. C.; Kurtz, D. A.; Huang, T.; Dempsey, J. L. Excited-State Proton-Coupled Electron Transfer: Different Avenues for Promoting Proton/Electron Movement with Solar Photons. *ACS Energy Letters*. 2017, **2**, 1246–1256.
6 Gagliardi, C. J.; Westlake, B. C.; Kent, C. A.; Paul, J. J.; Papanikolas, J. M.; Meyer, T. J. Integrating Proton Coupled Electron Transfer (PCET) and Excited States. *Coord. Chem. Rev.* 2010, **254**, 2459–2471.
7 Esswein, A. J.; Nocera, D. G. Hydrogen Production by Molecular Photocatalysis. *Chem. Rev.* 2007, **107**, 4022–4047.
8 Dempsey, J. L.; Winkler, J. R.; Gray, H. B. Mechanism of H_2 Evolution from a Photogenerated Hydridocobaloxime. *J. Am. Chem. Soc.* 2010, **132**, 16774–16776.
9 Whittemore, T. J.; Xue, C.; Huang, J.; Gallucci, J. C.; Turro, C. Single-Chromophore Single-Molecule Photocatalyst for the Production of Dihydrogen Using Low-Energy Light. *Nat. Chem.* 2020, **12**, 180–185.
10 Esswein, A. J.; Veige, A. S.; Nocera, D. G. A Photocycle for Hydrogen Production from Two-Electron Mixed-Valence Complexes. *J. Am. Chem. Soc.* 2005, **127**, 16641–16651.
11 Stiegman, A. E.; Stieglitz, M.; Tyler, D. R. Mechanism of the Low-Energy Photochemical Disproportionation Reactions of $(H_5\text{-}C_5H_5)_2MO_2(CO)_6$. *J. Am. Chem. Soc.* 1983, **105**, 6032–6037.
12 Stiegman, A. E.; Tyler, D. R. Mechanism of the Photochemical Disproportionation Reaction of Decacarbonyldimanganese ($Mn_2(CO)_{10}$) with Nitrogen Donor Ligands. *Inorg. Chem.* 1984, **23**, 527–529.
13 Stiegman, A. E.; Tyler, D. R. Photochemical Disproportionation of $(MeCp)_2Mo_2(CO)_6$(MeCp = $H_5\text{-}CH_3C_5H_4$) by Halides. *J. Am. Chem. Soc.* 1985, **107**, 967–971.
14 Cahoon, J. F.; Kling, M. F.; Schmatz, S.; Harris, C. B. 19-Electron Intermediates and Cage-Effects in the Photochemical Disproportionation of $[CpW(CO)_3]_2$ with Lewis Bases. *J. Am. Chem. Soc.* 2005, **127**, 12555–12565.
15 Cahoon, J. F.; Kling, M. F.; Sawyer, K. R.; Frei, H.; Harris, C. B. 19-Electron Intermediates in the Ligand Substitution of $CpW(CO)_3$ · with a Lewis Base. *J. Am. Chem. Soc.* 2006, **128**, 3152–3153.
16 Avey, A.; Tenhaeff, S. C.; R Weakley, T. J.; Tyler, D. R. Organometalllc Photochemistry in Aqueous Solution. Synthesis, Crystal and Molecular Structure, and Photochemistry of the $(\eta^5\text{-}C_5H_4COOH)_2W_2(CO)_6$ Complex. Generation of 19-Electron Organometalllc Complexes in Aqueous Solution and Their Use As. *Organometallics* 1991, **10**, 3607–3613.
17 Barry, J. T.; Tyler, D. R. Solvent Cage Effects: A Comparison of Geminate and Nongeminate Radical Cage Pair Combination Efficiencies. *Inorg. Chem.* 2020, **59,** 13875–13879.
18 ling, M. F.; Cahoon, J. F.; Glascoe, E. A.; Shanoski, J. E.; Harris, C. B. The Role of Odd-Electron Intermediates and in-Cage Electron Transfer in Ultrafast Photochemical Disproportionation Reactions in Lewis Bases. *J. Am. Chem. Soc.* 2004, **126**, 11414–11415.
19 Li, C.; Gao, F.; Cheng, S.; Tjahjono, M.; Van Meurs, M.; Tay, B. Y.; Jacob, C.; Guo, L.; Garland, M. From Stoichiometric to Catalytic Binuclear Elimination in Rh-W Hydroformylations. Identification of Two New Heterobimetallic Intermediates. *Organometallics* 2011, **30,** 4292–4296.
20 Cheng, T. Y.; Szalda, D. J.; Zhang, J.; Bullock, R. M. Synthesis and Structure of CpMo(CO)(Dppe)H and Its Oxidation by Ph 3C +. *Inorg. Chem.* 2006, **45**, 4712–4720.
21 McCarthy, B. D.; Dempsey, J. L. Decoding Proton-Coupled Electron Transfer with Potential-PKa Diagrams. *Inorg. Chem.* 2017, **56**, 1225–1231.
22 Van Der Eide, E. F.; Yang, P.; Walter, E. D.; Liu, T.; Bullock, R. M. Dinuclear Metalloradicals Featuring Unsupported Metal-Metal Bonds. *Angew. Chemie - Int. Ed.* 2012, **51**, 8361–8364.
23 Tilset, M. Oxidation of $CpM(CO)_3^{\bullet}$ and $CpM(CO)_3(NCMe)^{\bullet}$ (M = Cr, Mo, W): Kinetic and Thermodynamic Considerations of Their Possible Involvement as Reducing Agents. Relative Acetonitrile Affinities of $CpM(CO)_3^{+}$ and $CpM(CO)_3^{\bullet}$.. *Inorg. Chem.* 1994, **33**, 3121–3126.
24 Barbini, D. C.; Tanner, P. S.; Francone, T. D.; Furst, K. B.; Jones, W. E. Direct Electrochemical Investigations of 17-Electron Complexes of $CpM(CO)_3^{\bullet}$ (M = Mo, W, and Cr). *Inorg. Chem.* 1996, **35**, 4017–4022.
25 Ryan, O. B.; Tilset, M.; Parker, V. D. Chemical and Electrochemical Oxidation of Group 6 Cyclopentadienylmetal Hydrides. First Estimates of 17-Electron Metal-Hydride Cation-Radical Thermodynamic Acidities and Their Decomposition of 17-Electron Neutral Radicals. *J. Am. Chem. Soc* 1990, **112**, 2618–2626.
26 Gibson, D. H.; Owens, K.; Mandal, S. K.; Sattich, W. E.; Franco, J. O. *Synthesis and Thermolysis of Neutral Metal Formyl Complexes of Molybdenum, Tungsten, Manganese, and Rhenium*; *Organometallics* 1989, 8, 2, 498–505.
27 Patil, H. R.; G Graham, W. A. Organometallic Compounds with Metal-Metal Bonds. I. Tricarbonyl-π-Cyclopentadienylchromium, -Molybdenum, and -Tungsten Bonded to Methyl and Phenyl Derivatives of Germanium, Tin, and Lead. *Inorg. Chem.* 1966, **5**, 1401–1405.
28 Huang, T.; Rountree, E. S.; Traywick, A. P.; Bayoumi, M.; Dempsey, J. L. Supporting Info for Switching between Stepwise and Concerted Proton-Coupled Electron Transfer Pathways in Tungsten Hydride Activation. *J. Am. Chem. Soc.* 2018, **140**, 14655–14669.
29 Frisch, M. J.; Trucks, G. W.; Schlegel, H. B.; Scuseria, G. E.; Robb, M. A.; Cheeseman, J. R.; Scalmani, G.; Barone, V.; Petersson, G. A.; Nakatsuji, H.; Li, X.; Caricato, M.; Marenich, A. V.; Bloino, J.; Janesko, B. G.; Gomperts, R.; Mennucci, B.;

Hratch, D. J. Gaussian 16, Revision C.01. Gaussian, Inc.: Walingford CT 2016.
30 Cramer, C. J.; Truhlar, D. G. Density Functional Theory for Transition Metals and Transition Metal Chemistry. *Phys. Chem. Chem. Phys.* 2009, **11**, 10757–10816.
31 Petersson, G. A.; Tensfeldt, T. G.; Montgomery, J. A. A Complete Basis Set Model Chemistry. III. The Complete Basis Set-quadratic Configuration Interaction Family of Methods. *J. Chem. Phys.* 1991, **94**, 6091.
32 Wadt, W. R.; Hay, P. J. Ab Initio Effective Core Potentials for Molecular Calculations. Potentials for Main Group Elements Na to Bi. *J. Chem. Phys.* 1985, **82**, 284.
33 Wrighton, M. S.; Ginley, D. S. Photochemistry of Metal-Metal Bonded Complexes. III. Photoreactivity of Hexacarbonylbis(H_5-Cyclopentadienyl)Dimolybdenum(I) and -Ditungsten(I). *J. Am. Chem. Soc.* 1975, **97**, 4246–4251.
34 Levenson, R. A.; Gray, H. B.; Ceasar, G. P. Electronic and Vibrational Spectroscopy in a Nematic Liquid Crystal Solvent. Band Polarizations for Binuclear Metal Carbonyls. *J. Am. Chem. Soc.* 1970, **92**, 3653–3658.
35 Stiegman, A. E.; Tyler, D. R. Photochemical Disproportionation of Metal-Metal Bonded Carbonyl Dimers. *Coord. Chem. Rev.* 1985, **63**, 217–240.
36 Stiegman, A. E.; Tyler, D. R. Mechanism of the Photochemical Disproportionation Reactions of $(H_5\text{-}C_5H_5)_2M_2(CO)_6$ (M = Cr, Mo, W). *J. Am. Chem. Soc.* 1982, **104**, 2944–2945.